Cerebral Cortex, November 2020;30: 5885–5898

doi: 10.1093/cercor/bhaa164
Advance Access Publication Date: 18 June 2020
Original Article

ORIGINAL ARTICLE

Mapping the Brain-Wide Network Effects by Optogenetic Activation of the Corpus Callosum

Yi Chen[1,2], Filip Sobczak[1,2], Patricia Pais-Roldán[1,2], Cornelius Schwarz[3], Alan P. Koretsky[4] and Xin Yu[1,5]

[1]Research Group of Translational Neuroimaging and Neural Control, High-field Magnetic Resonance, Max Planck Institute for Biological Cybernetics, Tübingen, Baden-Württemberg 72076, Germany, [2]Graduate Training Centre of Neuroscience, University of Tübingen, Tübingen, Baden-Württemberg 72074, Germany, [3]Werner Reichardt Center for Integrative Neuroscience, Tübingen, Baden-Württemberg 72076, Germany, [4]Laboratory of Functional and Molecular Imaging, National Institute of Neurological Disorders and Stroke, Bethesda, MD 20892, USA and [5]Athinoula A. Martinos Center for Biomedical Imaging, Massachusetts General Hospital and Harvard Medical School, Charlestown, MA 02129, USA

Address correspondence to Dr Xin Yu. Email: xin.yu@tuebingen.mpg.de

Abstract

Optogenetically driven manipulation of circuit-specific activity enables causality studies, but its global brain-wide effect is rarely reported. Here, we applied simultaneous functional magnetic resonance imaging (fMRI) and calcium recording with optogenetic activation of the corpus callosum (CC) connecting barrel cortices (BC). Robust positive BOLD was detected in the ipsilateral BC due to antidromic activity, spreading to the ipsilateral motor cortex (MC), and posterior thalamus (PO). In the orthodromic target, positive BOLD was reliably evoked by 2 Hz light pulses, whereas 40 Hz light pulses led to reduced calcium, indicative of CC-mediated inhibition. This presumed optogenetic CC-mediated inhibition was further elucidated by pairing light pulses with whisker stimulation at varied interstimulus intervals. Whisker-induced positive BOLD and calcium signals were reduced at intervals of 50/100 ms. The calcium-amplitude-modulation-based correlation with whole-brain fMRI signal revealed that the inhibitory effects spread to contralateral BC, ipsilateral MC, and PO. This work raises the need for fMRI to elucidate the brain-wide network activation in response to optogenetic stimulation.

Key words: corpus callosum, fluorescent calcium, fMRI, interhemispheric inhibition, optogenetics

Introduction

The genetic expression of channelrhodopsin (ChR2) has been extensively applied to target specific cell types to ensure the activation of neuronal ensembles of interest (Nagel et al. 2002; Boyden et al. 2005; Li et al. 2005; Zhang et al. 2006). Optogenetic tools have revolutionized the strategy to perturb or manipulate the behavior of animals (Lima and Miesenbock 2005; Nagel et al. 2005; Adamantidis et al. 2007; Tsai et al. 2009). Interpretation of the linkage of brain function to specific behavioral readout relies on the assumed circuit-specific manipulation through in vivo optogenetic activation (Cardin et al. 2010; Carter et al. 2010; Tye and Deisseroth 2012; Kim et al. 2017). Optogenetic activation of numerous brain sites and defined neuronal populations in animals has been very successful in modulating behavior. However, there is a lack of systematic mapping of the result of specific modulation on brain-wide network activity, which may relay and affect the proposed link between function and behavior. Progress in this direction depends on the combined application of methods to simultaneously explore large-scale brain dynamics (Inoue et al. 2015; Bernal-Casas et al. 2017; Gao et al. 2019; Sych et al. 2019). One useful method for this purpose is functional magnetic resonance imaging (fMRI), which has been

successfully combined with optogenetics (Lee et al. 2010; Ryali et al. 2016; Yu et al. 2016; Albers, Schmid, et al. 2018a; Grandjean et al. 2019; Just and Faber 2019). We use here a method that adds GCaMP-mediated calcium recordings through an optical fiber for concurrent fMRI and neuronal calcium signal recording (Schulz et al. 2012; Schwalm et al. 2017; Albers, Wachsmuth, et al. 2018b; He et al. 2018; Wang et al. 2018). This multimodal cross-scale brain dynamic mapping scheme (fMRI, optogenetics and calcium recording) allows elucidating network activity upon circuit-specific optogenetic activation on the specific target level as well as across large brain regions (Schulz et al. 2012; Schmid et al. 2016; Albers, Schmid, et al. 2018a; Albers, Wachsmuth, et al. 2018b; He et al. 2018; Wang et al. 2018; van Alst et al. 2019).

Corpus callosum (CC), the major neural fiber bundles connecting the two hemispheres, plays a critical role in mediating the interhemispheric cortico-cortical connections (Sperry 1961; Gazzaniga 2005; Karolis et al. 2019). Despite the highly correlated structural anomalies of the CC with a wide range of disorders, for example, schizophrenia (Innocenti et al. 2003; Pomarol-Clotet et al. 2010), autism (Egaas et al. 1995; Anderson et al. 2011), epilepsy (Spencer et al. 1988; van Eijsden et al. 2011) and mental retardation (Schaefer and Bodensteiner 1999; van Schooneveld et al. 2011), CC-mediated neural mechanisms are primarily studied in loss-of-function models, such as split-brain/callosotomy or partial callosal lesion (Gazzaniga 2000, 2005; Schulte et al. 2010). To directly investigate the functional roles of callosal projections on regulating the interhemispheric excitatory-inhibitory balance, both in vitro and in vivo studies have applied microstimulation on one hemisphere or the callosal fiber bundles (Kawaguchi 1992; Kumar and Huguenard 2001; Hoffmeyer et al. 2007; Karayannis et al. 2007), or performed bilateral motor or sensory tasks in both human (Schnitzler et al. 1996; Ogawa et al. 2000; Ni et al. 2009; Bocci et al. 2011) and animal models (Ogawa et al. 2000; Shuler et al. 2001; Berwick et al. 2004; Wiest et al. 2005; Nemoto et al. 2012). Since the callosal fibers are reciprocally projecting to two hemispheres, bilateral, ortho- versus antidromically evoked neural activity has been difficult to disentangle. With optogenetic tools, the callosal projection neurons (CPNs) can be specifically (primarily) labeled with ChR2 from one hemisphere, enabling the unidirectional modulation of callosal activity (Petreanu et al. 2007; Palmer et al. 2013; Iordanova et al. 2018). The optogenetically driven callosal activity has been particularly helpful to disentangle interhemispheric inhibitory effects, for example, in the auditory cortex (Rock and Apicella 2015), prefrontal cortex (Lee et al. 2014), or hindlimb somatosensory cortex (Palmer et al. 2012). The goal of the present studies was to widen the view beyond the target-specific excitatory–inhibitory regulation by using a multimodal fMRI platform to characterize the global neural network activity upon optogenetic callosal activation.

In the present study, we implemented the multimodal fMRI platform with optogenetics to map the CC-mediated inhibition on the brain-wide network dynamics in three consecutive steps. First, we identified the antidromic versus orthodromic effect of CC-specific optogenetic stimulation. Optogenetic stimulation of callosal fibers connecting the barrel cortex (BC) to the other hemisphere revealed robust antidromic activation in the ipsilateral BC. In the orthodromic direction, both fMRI and neuronal calcium signals in the contralateral BC indicated strong depression of calcium signals with 40 Hz light pulses. Second, we specified the temporal characteristics of this presumptive CC-mediated inhibition on the thalamocortical activation to the BC. The optogenetic CC light pulses were paired with whisker stimulation electrical pulses at varying intervals from 0 to 200 ms in a randomized stimulation scheme. Significant inhibitory effects at 50 and 100 ms interval were detected by both fMRI and neural calcium recordings of the contralateral BC activated by whisker stimulation, but little difference was observed in the antidromically evoked fMRI signal in the ipsilateral BC. Thirdly, to further examine the brain-wide activity regulation upon paired optogenetic and whisker stimulation, the concurrent evoked-calcium signals in the contralateral BC were real-time detected at varying conditions and correlated with whole-brain fMRI signals. Besides the contralateral BC, the homologous ventral part of the ipsilateral BC, the motor cortex (MC) and posterior thalamus (PO) from the same side of the contralateral BC were detected in the correlation maps, showing amplitude modulation (AM) by CC-mediated inhibition at varied time intervals. This study not only specifies the optogenetically driven CC-mediated regulation of the local excitation/inhibition balance but also depicts the power of multimodal fMRI to characterize the brain-wide network activity associated with circuit-specific optogenetic activations in vivo. It highlights a vital aspect of the brain-wide activity for circuit-specific causality studies with optogenetic tools.

Materials and Methods

Animal Procedures

The study was performed in accordance with the German Animal Welfare Act (TierSchG) and Animal Welfare Laboratory Animal Ordinance (TierSchVersV). This is in full compliance with the guidelines of the EU Directive on the protection of animals used for scientific purposes (2010/63/EU). The study was reviewed by the ethics commission (§15 TierSchG) and approved by the state authority (Regierungspräsidium, Tübingen, Baden-Württemberg, Germany). A 12–12 h on/off lighting cycle was maintained to assure undisturbed circadian rhythm. The food and water were obtainable ad libitum. A total of 24 (17 for fMRI and 7 for electrophysiology) male Sprague–Dawley rats were used in this study.

Viral Injection

Intracerebral viral injection was performed in 4-week-old rats to express the viral vectors containing the light-sensitive protein channelrhodopsin-2 (ChR2, for optogenetics) and/or the calcium-sensitive protein (GCaMP, for calcium recording) in neurons. The construct AAV5.Syn.GCaMP6f.WPRE.SV40 was used to express GCaMP in the left BC and the constructs AAV5.CaMKII.hChR2(H134R)-mCherry.WPRE.hGH was used to express ChR2 in the right BC. The stereotaxic coordinates of the injections were 2.5 mm posterior to Bregma, 5 mm bilateral to the midline, 0.8–1.4 mm below the cortical surface. Rats were anesthetized with 1.5–2% isoflurane via nose cone and placed on a stereotaxic frame, an incision was made on the scalp and the skull was exposed. Craniotomies were performed with a pneumatic drill so as to cause minimal damage to cortical tissue. A volume of 0.6–0.9 and 0.6 µL, for optogenetics and calcium signal recording, respectively, was injected using a 10 µL syringe and 35-gauge needle. The injection rate was controlled by an infusion pump (Pump 11 Elite, Harvard Apparatus, USA). After injection, the needle was left in place for approximately 5 min before being slowly withdrawn. The craniotomies were

sealed with bone wax and the skin around the wound was sutured. Rats were subcutaneously injected with antibiotic and painkiller (Baytril and Flunixin) for three consecutive days to prevent bacterial infections and relieve postoperative pain after virus injection, at least 4 weeks before the acute experiment.

Immunohistochemistry

To verify the phenotype of the transfected cells, opsin localization, and optical fiber placement, perfused rat brains were fixed overnight in 4% paraformaldehyde and then equilibrated in 15% and 30% sucrose in 0.1 M PBS at 4 °C. About 30 µm-thick coronal sections were cut on a cryotome (CM3050S, Leica, Germany). Free-floating sections were washed in PBS, mounted on microscope slides, and incubated with DAPI (VectaShield, Vector Laboratories, USA) for 30 min at room temperature. Wide-field fluorescent images were acquired using a microscope (Zeiss, Germany) for assessment of GCaMP and ChR2 expression in BC. Digital images were minimally processed using ImageJ to enhance brightness and contrast for visualization purposes.

Optical Setup for Calcium Recordings

A laser was used as excitation light source (OBIS 488LS, Coherent, Germany) with a heat sink to enable laser operation throughout the entire specified temperature range from 10 to 40 °C. The light passed through a continuously variable neutral density filter (NDC-50C-2M-B, Thorlabs, Germany) and was reflected on a dichroic beam splitter (F48-487, AHF analysentechnik AG, Germany). The beam was collected into an AR coated achromatic lens (AC254-030-A, Thorlabs, Germany) fixed on a threaded flexure stage (HCS013, Thorlabs, Germany) mounted on an extension platform (AMA009/M, Thorlabs, Germany) of a fiber launch system (MAX350D/M, Thorlabs, Germany). The laser beam was projected into the fiber and propagated to its tip. The fluorescence emitted by neurons was collected through the fiber tip, propagated back and collimated by the achromatic lens, passed through the dichroic beam splitter and filtered by a band-pass filter (ET525/50 M, Chroma, USA) and focused by an AR-coated achromatic lens (AC254-030-A, Thorlabs, Germany). A silicon photomultiplier module (MiniSM 10 035, SensL, Germany) was applied to detect the emitted fluorescence. The entire optical system was enclosed in a light isolator box. The photomultiplier output was amplified (gain = 100) by a voltage amplifier (DLPVA-100-BLN-S, Femto, Germany), digitized, and detected by BIOPAC system (MP150 System, BIOPAC Systems, USA).

Animal Preparation and Fiber Optic Implantation for fMRI

Anesthesia was first induced in the animal with 5% isoflurane in the chamber. The anesthetized rat was intubated using a tracheal tube and a mechanical ventilator (SAR-830, CWE, USA) was used to ventilate animals throughout the whole experiment. Femoral arterial and venous catheterization was performed with polyethylene tubing for blood sampling, drug administration, and constant blood pressure measurements. After the surgery, isoflurane was switched off, and a bolus of the anesthetic alpha-chloralose (80 mg/kg) was infused intravenously. A mixture of alpha-chloralose (26.5 mg/kg/h) and pancuronium (2 mg/kg/h) was constantly infused to maintain the anesthesia and reduce motion artifacts.

Before transferring the animal to the MRI scanner, two craniotomies were performed: one for fixed fiber implantation to record calcium signals from BC, and the other one for dynamic insertion of the optical fiber to stimulate the CC using optogenetics (dynamic insertion was achieved by using a remote positioning tool (Chen et al. 2019)). The animal was placed on a stereotaxic frame, the scalp was opened and two ~1.5 mm diameter burr holes were drilled on the skull. The dura was carefully removed and an optical fiber with 200 µm core diameter (FT200EMT, Thorlabs, Germany) was inserted into the BC, at coordinates: 2.75–3.3 mm posterior to Bregma, 5.0 mm lateral to the midline, and 1.2–1.4 mm below the cortical surface. An adhesive gel was used to secure the calcium recording fiber to the skull above the dura. The craniotomy for optogenetics on CC in the other hemisphere, at coordinates: 2.75–3.3 mm posterior to Bregma, 1.8–2.4 mm lateral to the midline, was covered by agarose gel for the robotic arm-driven fiber insertion inside the MRI scanner. The eyes of the rats were covered by black light proof tapes to prevent stimulation of the visual system during the optogenetic fMRI, which may occur in cases with imperfect coverage or under the strong power of light pulses through tissue.

Functional MRI Acquisition

All images were acquired with a 14.1 T/26 cm horizontal bore magnet interfaced to an Avance III console and equipped with a 12 cm gradient set capable of providing 100 G/cm over a time of 150 µs. A transceiver single-loop surface coil with an inner diameter of 22 mm was placed directly over the rat head to acquire anatomical and fMRI images. Magnetic field homogeneity was optimized first by global shimming for anatomical images and followed by FASTMAP shimming protocol for the EPI sequence. Functional images were acquired with a 3D gradient-echo EPI sequence with the following parameters: Echo Time 11.5 ms, Repetition Time 1.5 s, FOV $1.92 \times 1.92 \times 1.92$ cm, matrix size $48 \times 48 \times 48$, spatial resolution $0.4 \times 0.4 \times 0.4$ mm. For anatomical reference, the RARE sequence was applied to acquire 48 coronal slices with the same geometry as that of the fMRI images. The paradigm for each trial consisted of 360 dummy scans to reach steady-state, 10 prestimulation scans, 5 scans during stimulation (stimulation period 8 s), and 35 poststimulation scans with total 13 epochs and 15 epochs for refined stimulus design (See Stimulation Protocols).

For fMRI and electrophysiology studies, needle electrodes were placed on whisker pads of the rats, and electric pulses (333 µs duration at 1.5 mA repeated at 3 Hz for 4 s) were first used as stimulation to serve as a positive control for the evoked BOLD signal or local field potential (LFP–)/calcium signal. Once that reliable fMRI signals and calcium signals were observed in response to electrical stimulation, optical stimulation was performed. For optogenetic stimulation, square pulses of blue light (473 nm) were delivered using a laser (MBL-III, CNI, China) connected to the 200 µm core optical fiber (FT200EMT, Thorlabs, Germany) and controlled by Master 9 (Master-9, A.M.P.I., Israel) to deliver blue light pulses at 1–40 Hz, 1–20 ms pulse width with 2–8 s duration. The light intensity was tested before each experiment and was calibrated with a power meter (PM20A, Thorlabs, Germany) to emit 0.6–40 mW from the tip of the optical fiber for CC activation.

Table 1 The number of trials acquired for six conditions

	Rat#1	Rat #2	Rat #3	Rat #4	Rat #5	Rat #6
Trials	6	4	4	4	6	5
Acquiring time	79 min 30 s	53 min	53 min	53 min	79 min 30 s	66 min 15 s

Table 2 The number of trials acquired with refined stimulus design

	Rat#7	Rat #8	Rat #9	Rat #10 (LFP)
Trials	9	12	5	7
Acquiring time	137 min 15 s	183 min	76 min 15 s	106 min 45 s

Table 3 Light power for optogenetic stimulation

	L6	L6.5	L7	L7.5	L8	L8.5	L9	L9.5	L9.9	L10
Light power (mW)	2.6	5.4	9.2	13.2	17.6	23.7	29.2	35.3	39.9	>40

Stimulation Protocols

A 2 Hz, 8 s optogenetic stimulus train (O train; 16 pulses to the CC) was delivered preceding a conditioning whisker stimulus train (W train; same pulse parameters were used, 0.75–1.5 mA) while varying the time interval between stimuli (0, 10, 25, 50, 100, and 200 ms), or without a W train, in a single trial. These stimulation conditions were automatically executed using a laser (MBL-III, CNI, China) and a stimulator (A365 Stimulus Isolator, WPI, USA) triggered by a combination program provided by pulse generator (Master-9, A.M.P.I., Israel), which were precisely synchronized with the start time of the image acquisition sequence in each trial. Each trial consisted of the first fixed whisker only stimuli block (W) and 12 blocks randomized for six different conditions, W, O (opto only condition), WO, W50O, W100O, W200O, in total 13 min and 15 s for each trial. For refined interstimulus intervals design, first fixed whisker stimuli block (W) and 14 blocks randomized for seven different conditions were used: W, OW, O10W, O25W, O50W, O100W, and O200W, in total 15 min 15 s for each trial. Tables 1–3 show the number of continuous trials acquired in this study, as well as light power for optogenetic stimulation.

Simultaneous Calcium Recording with Electrophysiology

The anesthetic and surgical preparation procedures were similar to the fMRI experiments. For antidromic activity recording experiments in Figure 1 and Supplementary Figures 2–5, tungsten microelectrode (UEWSDDSMCN1M, FHC, USA) was implanted in the right BC to record the LFP from the CPNs. For orthodromic activity in Figure 2 and Supplementary Figures 7–10, the same kind of tungsten microelectrode was attached to the fiber optic closely, implanted in the left BC, then secured to the skull by an adhesive gel. To calculate the coordinates of optical fiber implantation for CC activation, a FLASH anatomical MRI image was acquired to confirm the virus injection 1 day before the experiment. The LFP was recorded and amplified through the EEG module of the BIOPAC system (gain factor, 5000, band-pass filter, 0.02–100 Hz, sampling rate, 5000/s). In parallel, the GCaMP6f-mediated fluorescent signal and blood pressure were digitized and recorded with BIOPAC (MP150 System, BIOPAC Systems, USA) at a sampling rate of 5 kHz. The experiment design and equipment used afterward were similar to the fMRI experiments.

Data Analysis

Acquired data were analyzed using Functional NeuroImages software (AFNI, NIH, USA) and custom-written Matlab (MATLAB, MathWorks, USA) programs for calcium signals. The fiber optical neuronal calcium signals were low-pass filtered at 100 Hz using zero-phase shift digital filtering (filtfilt function in MATLAB). The relative percentage change of fluorescence ($\Delta F/F$) was defined as $(F - F_0)/F_0$, where F_0 is the baseline, that is, the average fluorescent signal in a 2 s prestimulation window. For Figure 2*d*, the spike value is defined by the maximal value for the difference in $\Delta F/F$ in a time window 0.3 s after the stimulus, as shown from 40 Hz in Figure 2*c*, while the baseline drift is the average calcium signal from 0.3 to 8 s after the spike recovered to baseline for 40 Hz stimulation. For Figure 3*e*, the first epoch for each trial (fixed W condition) was excluded in the data analysis and the calcium signal was averaged for each condition from all the acquired trials for each animal. Each condition was then normalized by the maximum positive deflection of calcium signal alone conditions. For Figure 3*f*,*h*,*i*, the amplitude peak of the neuronal fluorescent signal in response to 8 s whisker stimulus was calculated as the maximal difference in $\Delta F/F$ in a time window 300 ms after stimulus, then normalized to the whisker only (W) condition (100%). The unnormalized amplitude for the difference in $\Delta F/F$ for each epoch was used to generate the calcium signal-based regressor (Supplementary Fig. 14) for fMRI correlation map in Figure 4.

For evoked fMRI analysis, EPI images were first aligned to anatomical images acquired in the same orientation with the same geometry. The anatomical MRI images were registered to a template across animals, as well as EPI datasets. The baseline signal of EPI images was normalized to 100 for statistical analysis of the multiple trials of EPI time courses. The time courses of the BOLD signal were extracted from regions of interest, for example, BC, MC, and PO, based on the brain atlas

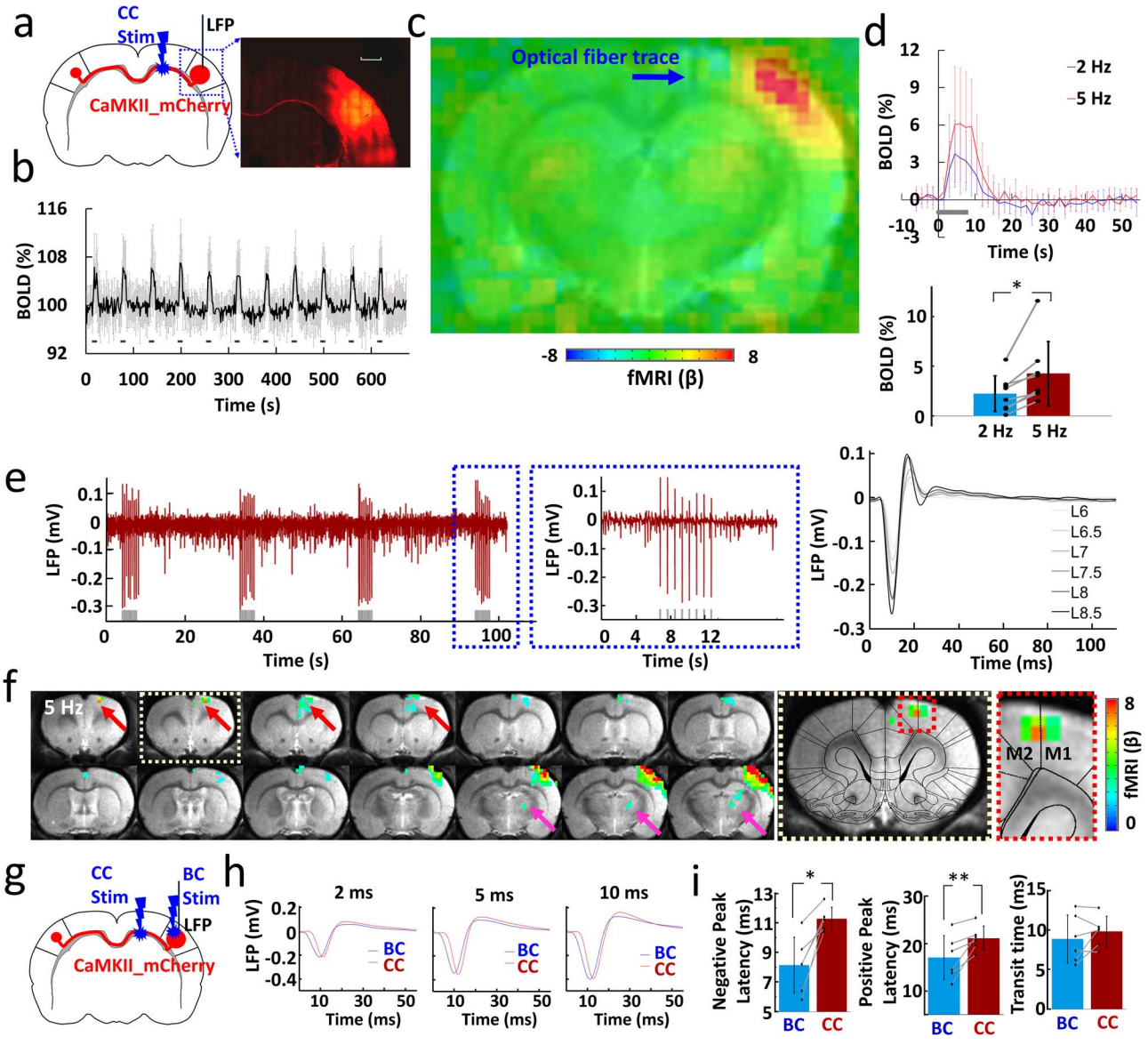

Figure 1. Antidromic activation upon CC optogenetic stimulation. (*a*) Left: schematic of experimental design. Right: representative wide-field fluorescence image illustrating the robust expression of ChR2-mCherry at the injection site (right BC) and along the CC. Medial is to the left. Red, AAV5.CaMKII.ChR2-mCherry. Scale bar, 1 mm. (*b*) Average time courses of fMRI signal changes in right BC ($n = 8$ animals) upon optogenetic stimulation. Error bars represent mean ± SD. (*c*) Averaged fMRI map showing the strong antidromic activation in BC in the right hemisphere with fiber optic trace (blue arrow) during optogenetic stimulation of CC from eight rats of block design: 8 s on/52 s off, 11 epochs, 10 ms light pulse, 5 Hz. (*d*) Top: averaged BOLD signals upon different stimulation frequencies (2 Hz in blue, 5 Hz in red). Error bars represent mean ± SD. Lower: mean amplitudes of the BOLD signals (0–10.5 s) for 2 and 5 Hz ($n = 8$, paired *t* test, $^{*}P = 0.006$). Error bars represent mean ± SD. (*e*) Left: the representative LFP for antidromic activation (gray lines, light pulses). Right: laser power dependent LFPs (pulse width, 10 ms). (*f*) Representative BOLD map showing the activity in the projected MC (red arrows) and PO (magenta arrow) from the antidromic activity in the BC. Dashed boxes showed the enlarged view of projected MC (GLM-based *t*-statistics in AFNI is used. *P* (corrected) = 0.0319). (*g*) Schematic of experimental design. (*h*) The representative LFP for direct BC light stimulation (blue) and antidromic activation (red) recorded with light pulse durations of 2, 5, and 10 ms. (*i*) The different peak latency and transit time for the LFP induced by CC and BC light stimulation ($n = 6$ animals, paired *t* test, $^{*}P = 0.002$, $^{**}P = 0.009$, pulse width, 10 ms). Error bars represent mean ± SD.

and activation or correlation values. The BOLD amplitude for each condition was defined as the average value for the volumes within the 0–10.5 s following the onset of stimulation (when stimulation duration was 8 s). The hemodynamic response function (HRF) used was the default block function of the linear program 3dDeconvolve in AFNI. BLOCK (L, 1) computes a convolution of a square wave of duration L and makes a peak amplitude of block response = 1, with $g(t) = t^4e^{-t}/[4^4e^{-4}]$ (peak value = 1). In this case, each beta weight represents the peak height of the corresponding BLOCK curve for that class, that is, the beta weight is the magnitude of the response to the entire stimulus block, as shown in Figures 1 and 3

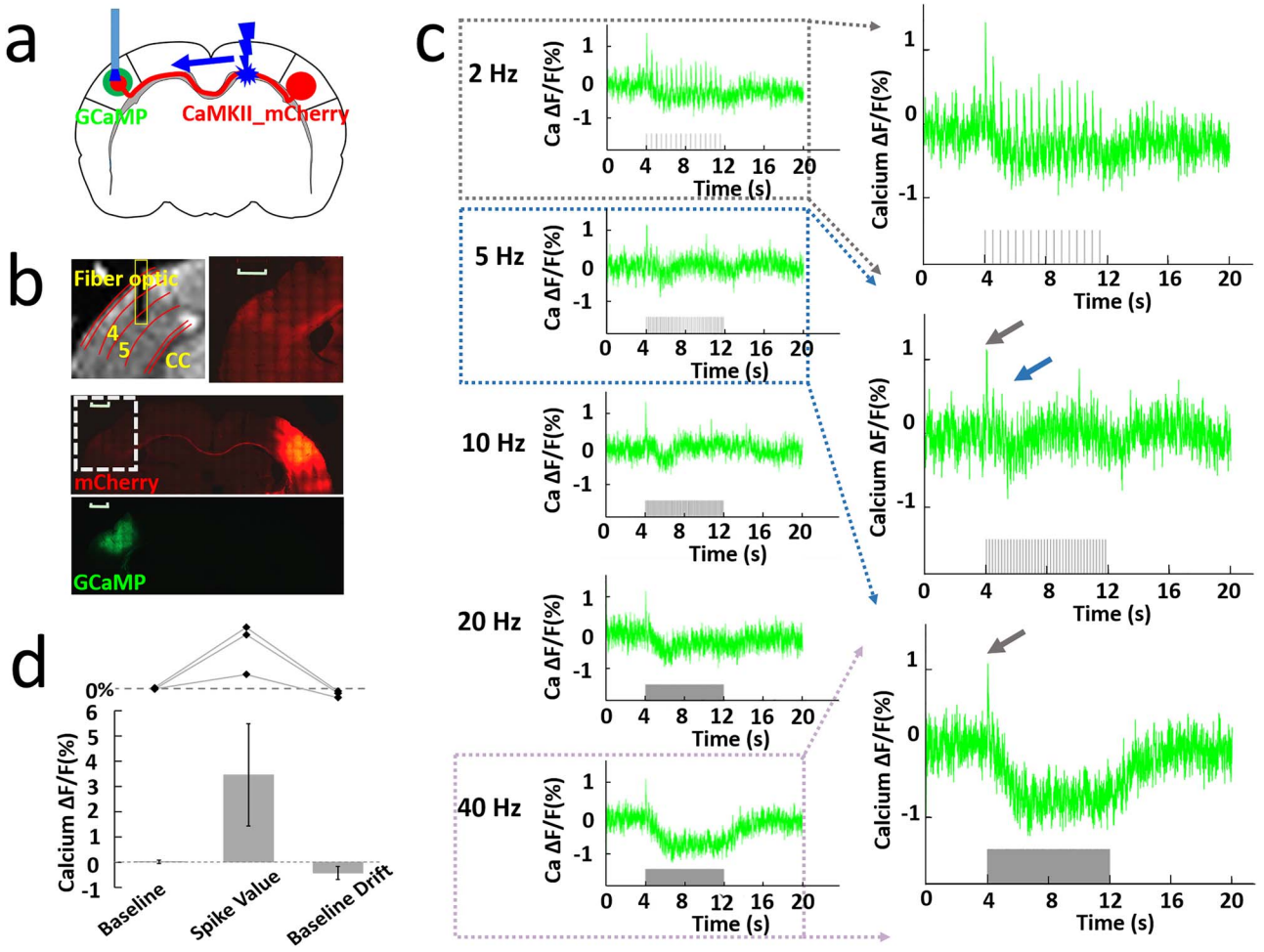

Figure 2. Orthodromic activation upon CC optogenetic stimulation. (*a*) Schematic of experimental design. (*b*) Top left: representative RARE anatomical image used to identify the optical fiber location for calcium signal recording in the layer V of BC. Top right: enlarged immunostaining image illustrating the ChR2-mCherry expression in the left hemisphere (opposite to the injection site, white dashed box below). Middle: representative wide-field fluorescence image illustrating robust ChR2-mCherry at the injection site (right BC) and along the axonal fibers to the other hemisphere. Red, AAV5.CaMKII.ChR2-mCherry. Bottom: the immunostaining image illustrating robust GCaMP6f expression (green) in the left BC. Scale bar, 1 mm. (*c*) Left: representative calcium signal changes upon 8 s of orthodromic activation responses to 2, 5, 10, 20, and 40 Hz stimulation. Right: enlarged calcium signal changes responses to 2, 5, and 40 Hz stimulation. (*d*) The analysis of calcium baseline, spike value (3.46 ± 2.03%), and baseline drift (−0.43 ± 0.26%) from three animals. Error bars represent mean ± SD.

and Supplementary Figure 1. The HRF model is defined as follows:

$$\mathrm{HRF}(t) = \mathrm{int}\left(g\left(t-s\right), s = 0..\min\left(t, L\right)\right)$$

For correlation analysis, a calcium signal amplitude modulated regressor (AM2) based AFNI BLOCK (L, 1) function was used (Supplementary Fig. 14). The regressor for amplitude modulated response model is as follows:

$$r_{\mathrm{AM2}}(t) = \sum_{k=1}^{K} h\left(t-\tau_k\right) \bullet \left(a_k - \bar{a}\right)$$

where a_k is the value of kth auxiliary behavioral information (ABI) value, that is, calcium amplitude value for the difference in $\Delta F/F$ for each epoch, and $\bar{a}$ is the average calcium amplitude value for all the epochs for the individual animal. The statistics and β for the AM2 regressor make activation map of places whose BOLD response changes with changes in ABI, that is, the changes in calcium signals for each epoch. This allows separation of voxels that are active but are not detectably modulated by the ABI from voxels that are ABI-sensitive. In contrast to AM2-based analysis, the AM1 regressor cannot distinguish the evoked versus modulated effects as described in Supplementary Figure 15. Thus, the AM2-based regression is applied for analysis.

Results

Antidromic Activation by Callosal Optogenetic Stimulation

By injecting the AAV-ChR2 viral vectors into the BC of rats, ChR2 can be expressed in CPNs, in particular through their axonal fiber bundles projecting to the contralateral BC (Fig. 1*a*) (Petreanu et al. 2007; Xin Yu and Koretsky 2013). Based on our previous work (Chen et al. 2019), an MRI-guided robotic arm was used to provide high flexibility to insert the optical fiber and sufficient targeting accuracy of the ~200 μm callosal fiber bundle for multimodal fMRI. The most salient BOLD fMRI signal evoked

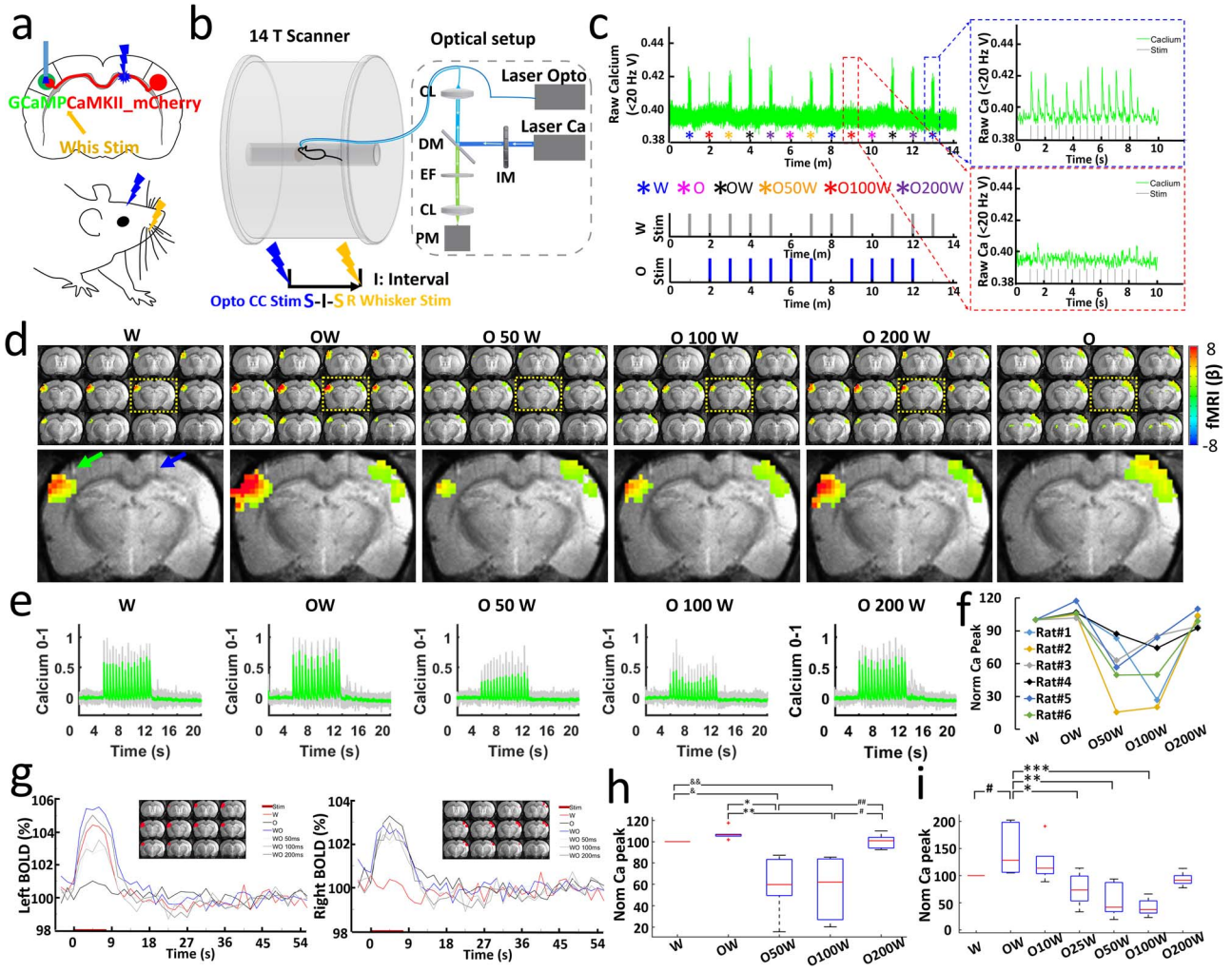

Figure 3. Simultaneous measurement of BOLD and calcium signals during CC optogenetic stimulation and electrical whisker stimulation with varying time intervals. (*a*) Stimulation scheme. There are six conditions, whisker stimuli only (W), CC stimuli only (O), CC stimuli and whisker stimuli together (OW), CC stimuli and 50, 100, 200 ms delayed whisker stimuli (O50W, O100W, O200W). (*b*) Schematic drawing of the experimental setup to conduct optogenetic fMRI with simultaneous fiber-optic calcium recording. CL: coupling lens, DM: dichroic mirror, EF: emission filter, PM: photomultiplier, IM: intensity modulation. (*c*) Typical calcium signals for condition W (blue dash box) and O100W (red dash box) from a representative rat. (*d*) Top: averaged fMRI map of brain-wide activity for six conditions across six rats (GLM-based *t*-statistics in AFNI is used. *P* (corrected) < 0.01) of block design: 8 s on/52 s off, 13 epochs, 20 ms light pulse, 2 Hz, 5–39 mw. Bottom: enlarged brain slice showing the differences of BOLD mapping in BC in both hemispheres with fiber optic trace for optogenetic stimulation (blue arrow) and calcium recording fiber (green arrow). (*e*) Averaged normalized calcium signal in left BC, gray lines showing the individual normalized calcium signal from six rats (Trials # = 29, details see Methods, Table 1). (*f*) Normalized calcium signal for an individual rat as a function of conditions: W, OW, O50W, O100W, O200W. (*g*) Left: averaged BOLD changes in the ROI (red region on anatomical images) in the left BC induced by whisker stimulation. There is a slight increase for O condition, which is consistent with Supplementary Figure 6. Right: averaged BOLD changes in the ROI (red region on anatomical images) in the right BC induced by CC stimulation. (*h*) Averaged normalized calcium signal changes across six rats modulated by stimulus time intervals (ANOVA, $P < 0.01$). (*i*) Averaged normalized calcium signal changes across four rats modulated by stimulus time intervals (ANOVA, $P < 0.03$).

by CC optogenetic stimulation was detected at the ipsilateral BC housing the labeled CPN ($n = 8$ animals, Fig. 1*b*,*c*, 5 Hz light pulses). The antidromically evoked hemodynamic responses to 5 Hz stimulation were significantly stronger than the responses to 2 Hz (Fig. 1*d*). In addition, antidromic BOLD and LFP signal were evoked by systematically varying laser power, light pulse width, frequency, and duration of the optogenetic stimulation (Fig. 1*e*, Supplementary Figs 1 and 2). The fMRI analysis revealed widespread brain activation in the ipsilateral hemisphere, which likely originates from antidromic CPN activity spread by multi-synaptic pathways to the MC and PO (Fig. 1*f*). These widespread ipsilateral effects were readily seen with the 5 Hz stimulation paradigm but could not be evoked using lower stimulation frequencies.

Next, we examined the temporal characteristics of the antidromic activity. In general, CC-mediated antidromic LFP responses in BC to different pulse widths and frequencies were similar to the responses observed when BC was directly activated (Supplementary Figs 3 and 4). Likewise, the whole-brain BOLD signal showed time courses and distributions as reported earlier with direct BC stimulation (Yu et al. 2012, 2016). We were concerned that the stimulation light could

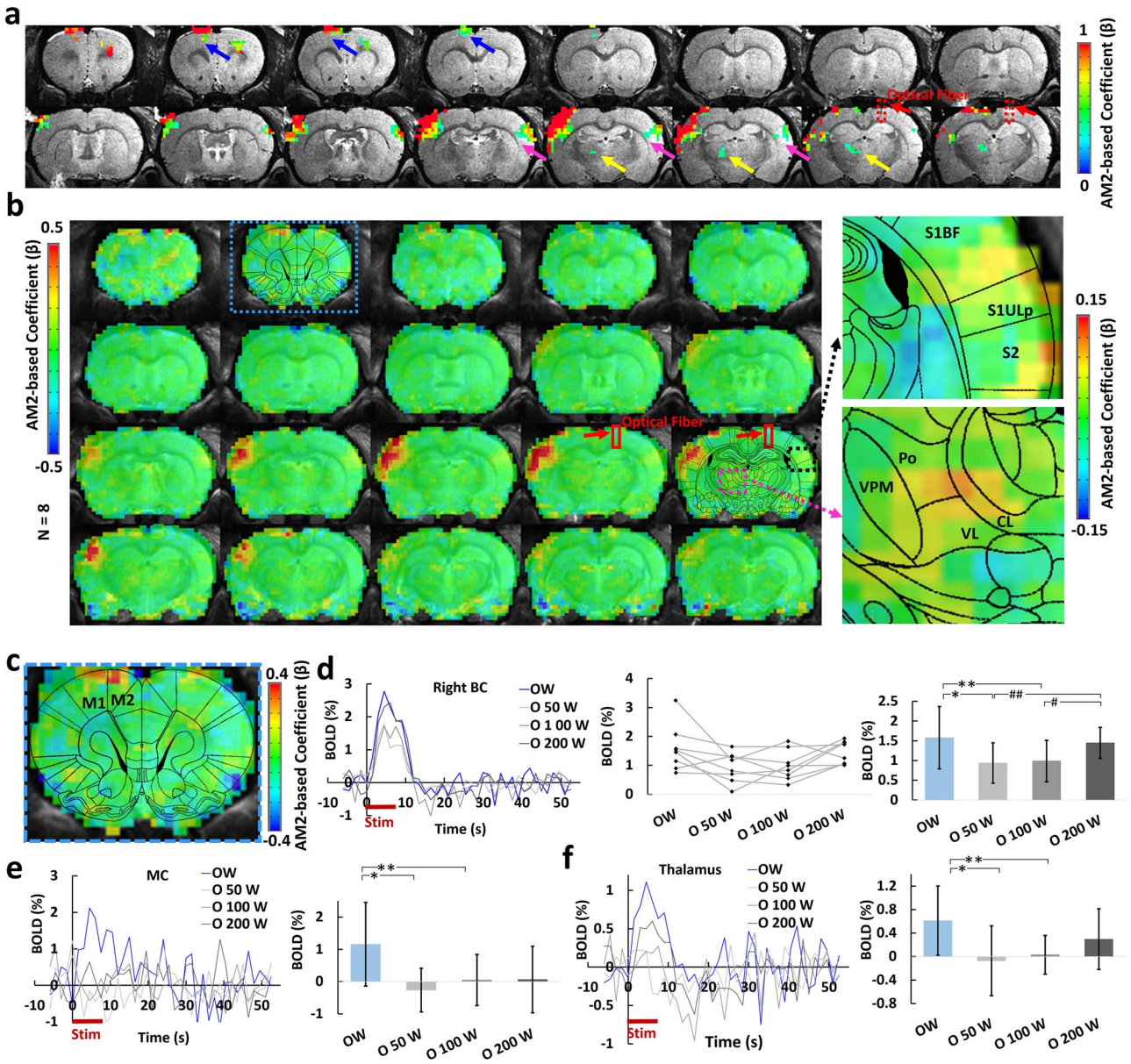

Figure 4. Calcium AM-based whole brain BOLD correlation analysis. (*a*) one representative animal map overlaid on the anatomical image with a statistical threshold (*P* (corrected) < 0.05, cluster size >15 voxels, MC, blue arrows, BC, magenta arrows, PO, yellow arrows, optical fiber trace, red arrows). (*b*) Group-averaged correlation maps show the spatial distribution of the positive correlation located at left BC, MC, as well as the PO by overlying with the brain atlas (red square, optical fiber traces, right panel: the enlarged images of the correlation map overlaid on the brain atlas). (*c*) Enlarged correlation map shows the positive correlation at the MC. (*d*) Left: averaged time courses from the right BC at different conditions ($n = 8$ rats). Middle: mean amplitudes of the BOLD signals (0–10.5 s) for individual rats. Right: averaged amplitudes of the BOLD signals (0–10.5 s, mean ± SD, ANOVA, $^{*}P = 0.027$, $^{**}P = 0.004$, $\#P = 0.030$, $\#\#P = 0.003$). (*e*) Left: averaged time courses from the MC ($n = 8$ rats). Right: averaged amplitudes of the BOLD signals (0–10.5 s, mean ± SD, ANOVA, $^{*}P = 0.005$, $^{**}P = 0.01$). (*f*) Left: averaged time courses from the PO ($n = 8$ rats). Right: averaged amplitudes of the BOLD signal (0–10.5 s, mean ± SD, ANOVA, $^{*}P = 0.009$, $^{**}P = 0.012$). W: whisker stimulation only, OW: simultaneous optical and whisker stimulation, O[x]W optical stimulation followed by [x] ms-delayed whisker stimulation.

have activated CPN directly in the BC. To test this concern, we recorded the LFPs evoked by optogenetic CC and direct BC stimulation in the same rat (Fig. 1*g*,*h*), and found that the latency of the response was systematically higher for CC as compared with BC stimulation (negative peak latency: BC: 8.13 ± 1.89 ms, CC: 11.27 ± 0.78 ms; positive peak latency: BC: 17.00 ± 4.65 ms, CC: 21.07 ± 2.60 ms; $n = 6$ animals, paired *t* test, $^{*}P = 0.002$, $^{**}P = 0.009$) (Fig. 1*i*). Otherwise the time course of the LFP response was similar, which showed, firstly that CC stimulation is likely stimulating the CC axons as intended, and secondly that BC is activated in a very similar way by CPNs as with direct stimulation. In support of this conclusion, we found that optogenetically activating callosal fibers from the other hemisphere (opposite to the virus injection site) readily showed latency differences (Supplementary Fig. 5), as expected from the axonal conduction delays of the transmission of the electrical impulses (Simmons and Pearlman 1983; Caminiti et al. 2013).

Orthodromic Activation by Callosal Optogenetic Stimulation

Compared with antidromically evoked activity, the BOLD signal in the contralateral hemisphere evoked by orthodromic stimulation was smaller, and the stimulus–response relationship was different. For instance, quite different from the antidromic situation, the BOLD signal observed with 2 Hz optogenetic CC stimulation was stronger than that with 5 Hz (Supplementary Fig. 6). To investigate the CC-mediated corticocortical interaction in the contralateral hemisphere, we injected the Syn-GCaMP6f and CaMKII-ChR2-mCherry into the left and right BC, respectively, and recorded both calcium and LFP signal upon optogenetic CC stimulation (Fig. 2*a*,*b*). Here we focused on layer 5 (Fig. 2*b*), because it is the main target lamina of CC projections (Suarez et al. 2014; Rock and Apicella 2015), as well as the main output layer of the BC (Fox 2008). Figure 2*c* shows the frequency-dependent orthodromic calcium signals from one representative rat. As mentioned before, evoked calcium transients appeared in a strict frequency-dependent fashion. A strong transient was detected following each light pulse at 2 Hz, while at higher frequencies, only the first pulse triggered a full-fledged calcium response (Fig. 2*c*). The subsequent pulse responses were depressed or missing entirely and gave way to a slow decrement in fluorescence (Fig. 2*c*). The decrement of Ca^{2+} signal was constantly present throughout the entire stimulus interval (see gray bar 40 Hz stimulation in Fig. 2*c*), and slowly relaxed back to baseline only after the end of stimulation. Simultaneous LFP and calcium recordings in a representative rat shared the same pattern, strengthening the notion of a strong suppression of responses at higher stimulus frequencies (Supplementary Fig. 7), and offering an explanation for the likewise decreased orthodromic BOLD signals at 5 Hz (Supplementary Fig. 6). The calcium baseline drift for 40 Hz was reproduced and was quantified in Fig. 2*d*, suggesting a highly robust corticocortical inhibition effect as previously reported by electrophysiological recording (Butovas and Schwarz 2003; Butovas et al. 2006; Lee et al. 2014). The evoked LFP and calcium signals dependence on the laser power, light pulse width, and duration provide strong evidence for reliable detection of the orthodromic activity (Supplementary Figs 8–10). It is noteworthy that the CC-mediated orthodromic activity shows different response patterns for both LFP/calcium and fMRI signals from the antidromic activity, indicating a distinct impact on the local excitation-inhibition balance through the CC-mediated inputs.

The CC-mediated Inhibitory Effects on the Sensory-evoked Cortical Activity

Next, we investigated the effect of CC-mediated suppression on sensory-evoked cortical activity. The optogenetic light pulse train ('O', 2 Hz, 16 pulses in 8 s) for CC optogenetic stimulation was delivered at time intervals of 0, 50, 100, and 200 ms after stimulating the primary afferents in the whisker pad with a microstimulation pulse train ('W', 2 Hz, 16 pulses). In total six conditions (W, O, OW, O50W, O100W, and O200W, OxW means optogenetic pulse precedes the whisker stimulation pulse by "x" ms) were delivered in trials of randomized order (Fig. 3*a*) using the multimodal fMRI platform (Fig. 3*b*). Typical raw calcium signals and stimulation design are shown in Fig. 3*c* with a W condition leading the other randomized 12 epochs (six conditions repeated twice in a randomized order). We found a strong suppression of BOLD in the orthodromic direction with latencies of 50 and 100 ms (Fig. 3*d*,*g*). The suppression was partially recovered at the O200W condition. This phenomenon was absent on the antidromic side (Fig. 3*g*). A similar picture emerged with averaged calcium signals recorded in layer 5 of the contralateral BC (Fig. 3*e*). Ca^{2+} signals and BOLD were highly correlated (Fig. 3*e*,*g*), showing reduced calcium percentage changes at O50W and O100W conditions across animals (Fig. 3*f*). Normalizing both signals to the whisker-only (W) condition (Supplementary Fig. 11), we found that the mean signal changes of BOLD from 100% (W) to 107.3%, 59.2%, 56.8%, and 100.4%, while the calcium signal changed from 100% (W) to 127.8%, 45.2%, 59.5% and 107.1% at conditions of OW, O50W, O100W, and O200W, respectively (Fig. 3*h*). To investigate the temporal features of the interaction on a more precise scale, we refined the stimulus intervals for whisker stimulation by adding 10 and 25 ms conditions (W, OW, O10W, O25W, O50W, O100W, and O200W) in another group of rats (Fig. 3*i* and Supplementary Fig. 12). Again similar patterns emerged as seen before (Fig. 3*i* and Supplementary Fig. 12). For O10W, no significant difference was observed in comparison with the OW condition, but the calcium responses at O25W were significantly lower than the OW condition (Supplementary Fig. 12). As reported from in vitro CC electrical stimulation studies by Kawaguchi et al. (Kawaguchi 1992), CC stimulation leads to two inhibitory postsynaptic potential (IPSP) peaks (the earlier peak at ~30 ms, and the later peak at ~180 ms), which could underlie the inhibitory effects at O25W and the later recovery at O200W to different extents. Furthermore, the simultaneous LFP and calcium recording confirmed the time-interval specific inhibitory effects by direct optogenetic CC stimulation to modulate the sensory-evoked cortical activity pattern in the BC (Supplementary Fig. 13). These results are consistent with results using whisker, forepaw, and visual stimulation in rodents and human studies (Schnitzler et al. 1996; Ogawa et al. 2000; Shuler et al. 2001; Berwick et al. 2004; Wiest et al. 2005; Ni et al. 2009; Bocci et al. 2011; Nemoto et al. 2012).

Global Network Mapping Based on the Optogenetically-driven CC-mediated Inhibitory Effects

The 3D fMRI data with concurrent calcium signal acquired at different conditions with CC and whisker stimulation allowed analyzing the global effect of the optogenetically driven CC-mediated inhibition. To this end, the calcium signal AM factor was applied to the ideal function produced by the general linear model (GLM), which was correlated with the 3D fMRI time course (Supplementary Fig. 14) (Cox 1996; Wang et al. 2018). As shown in Supplementary Figure 14, the calcium-AM2 regressor is derived from the stimulation-driven ideal function, of which the GLM analysis leads to an AM-specific correlation with the whole brain fMRI signal (an AM1-based regression method merges both evoked and modulated effects, detailed discussion is described in Methods and Supplementary Fig. 15). Thus, the calcium-based AM2-correlation with the entire brain generated a map of global brain dynamic changes related to specific CC-mediated inhibitory effect. The strongest correlation was found in the left BC (Fig 4). A positive correlation was further observed in the ipsilateral (left) MC and PO, which are projection targets of the BC, as well as the ventral right BC (Fig. 4*a*,*b*,*c*). We next extracted the time courses from the highlighted ROIs to examine the changes of the fMRI signals at different conditions. The averaged time courses from the right BC ROI reflected the patterns seen in the orthodromically affected BC before. In these

conditions (O50W and O100W), the BOLD signals of the left BC were reduced with respect to the other conditions (Fig. 4*d*). Similar patterns of BOLD responses were detected in the MC (Fig. 4*e*) as well as the PO (Fig. 4*f*) directly connected to the left BC. In particular, it has been shown that corticalthalamic projections from Layer 5 BC neurons highly innervate to the PO area (Sumser et al. 2017), establishing a potential feed-forward regulatory pathway to support the covaried CC-relevant BC-PO activity as presented in the AM2-based correlation maps. It is noteworthy that the positively correlated right BC area was not overlapping with cortical areas housing the CPNs (Fig. 3*d*). Thus, the AM2-based global correlation map presents unique CPN-mediated transcallosal regulation on sensory inputs, precluding the possibility that MC and PO might have integrated the callosal and sensory input independently of BC. In summary, these results demonstrate that the global network is modulated with the CC-specific evoked activity in BC.

Discussion

We have performed simultaneous BOLD-fMRI and calcium recording in combination with callosal-circuit specific optogenetic stimulation to map the brain-wide network activation. The robust BOLD signal due to the antidromic activity was detected in the ipsilateral BC, which also led to fMRI detection in the ipsilateral MC and PO region with the higher frequency stimulus. In contrast, the positive BOLD signal through the CC-orthodromic activity was only reliably observed at the lower frequency optogenetic stimulus. With the 40-Hz light pulses, the calcium baseline suppression was detected and interpreted to be due to the CC-mediated cortico-cortical inhibitory effect. To further test this, CC-mediated inhibition was further paired with the whisker stimulation paradigm at varying interstimulus intervals from 0 to 200 ms, showing significant suppression at the O50W and O100W conditions in the left BC by the concurrent fMRI and calcium recording. By extracting the event-dependent calcium peak amplitudes at varied conditions as a regressor, an AM-based correlation map revealed brain-wide inhibitory effects spreading through the ventral border of the right BC and the left MC and PO. Thus, the multimodal fMRI platform provides thorough brain-wide network activation maps for the CC-specific optogenetic stimulation.

The observation of strong antidromic propagation by callosal optogenetic stimulation and related synaptic spread of activity presents a caveat for the conclusion of circuit specificity for in vivo optogenetic studies. In particular, when fibers projecting to specific functional nuclei are optogenetically activated, possible spreading network activity from the antidromically activated brain sites needs to be considered. In our experiments, BOLD signals were detected in both MC and PO, which receive afferents from the antidromically activated BC (at 5 Hz light pulses), indicating a (for the experimental purpose unintended) widespread optogenetic activation pattern in the brain-wide network (Fig. 1*e*). This spread is likely due to synaptic propagation via activated local or regional axon collaterals of CPNs (Wilson 1987; White and Czeiger 1991; Cauller et al. 1998; Mitchell and Macklis 2005; Fame et al. 2011). For the present spread into motor and sensorimotor structures, deep layer CPNs with long-range projections into sensorimotor brain areas are likely involved (Veinante and Deschenes 2003). In addition, multisynaptic pathways, involving either cortico-cortical or cortico-thalamic projections may have contributed to the spread brain-wide activation (Kleinfeld and Deschenes 2011; Gambino et al. 2014). In conclusion, it is mandatory to consider brain-wide activation patterns, even in case of application of highly circuit-specific optogenetic activation schemes.

Certainly, the optogenetic callosal activation also elicits specific unidirectional callosal orthodromic activity, as shown in earlier reports (Kawaguchi 1992; Hoffmeyer et al. 2007; Karayannis et al. 2007). Optogenetic activation of the callosal projection terminals in brain slices led to better characterization of the excitatory and inhibitory circuit regulation by callosal inputs (Petreanu et al. 2007; Palmer et al. 2012; Lee et al. 2014; Rock and Apicella 2015; Petrus et al. 2019). Our observations further support the nonlinear neurovascular coupling events observed with optical intrinsic signal measurements and laser-doppler flowmetry upon optogenetic or electrical CC stimulation (Hoffmeyer et al. 2007; Iordanova et al. 2018). In our study, the fact that orthodromic BOLD signals were readily observed with low-frequency stimulation (2 Hz) but strongly reduced at higher frequency (5 Hz), reveals a critical nonlinear manner of the hemodynamic responses driven by the CC-mediated neuronal activation(Fig. 1*f* and 2*c*, and Supplementary Fig. 6). Future studies should incorporate the line-scanning fMRI to investigate the CC-mediated neurovascular coupling with different stimulation frequencies, in particular, to elucidate the laminar-specific fMRI signal changes to 40 Hz stimulation when conventional EPI–fMRI does not detect reliable negative BOLD signal changes. We show here that peripheral whisker stimulation is well suited to study the suppressive effects of orthodromically conveyed activity specific to the callosum, which is not possible using in vivo bilateral stimulation paradigms in rodents (Ogawa et al. 2000; Shuler et al. 2001; Berwick et al. 2004; Wiest et al. 2005; Nemoto et al. 2012) or bilateral motor or visual tasks in humans (Schnitzler et al. 1996; Ni et al. 2009; Bocci et al. 2011) where other pathways may be involved. In particular, CC-induced orthodromic activity of L5 pyramidal neurons evoked a calcium transient followed by marked depression of calcium signals responding to light pulses on CC (Fig. 2*c*,*d*) (consistent with the optogenetic results in brain slices (Lee et al. 2014)). Electrophysiology in brain slices has elucidated that CC-mediated glutamatergic excitatory postsynaptic potentials are followed by early $GABA_A$- and late $GABA_B$-mediated IPSPs lasting for several hundred milliseconds (Kawaguchi 1992; Kumar and Huguenard 2001; Karayannis et al. 2007; Palmer et al. 2012), strongly suggesting that the depression seen here is partly due to bi-synaptic inhibition. Also, while when pairing callosal activation with 2 Hz whisker stimulation, the cortical response time course shows a depressive effect around 50–100 ms, of which the interval fits the previous finding that local intracortical activation is accompanied by activation of long-lasting synaptic GABAergic inhibition (Butovas and Schwarz 2003; Butovas et al. 2006; Cardin et al. 2009; Logothetis et al. 2010; Moore et al. 2010; Palmer et al. 2013). It is also noteworthy that the ChR2 is specifically expressed in the excitatory CPNs with the CaMKII promoter, which eliminates the contribution from the direct GABAergic callosal projections to inhibit the local neuronal activity (Bitzenhofer et al. 2017; Rock et al. 2018). Alternatively, it remains unclear whether the callosal-activated inhibitory interneurons could directly modulate the ascending thalamocortical terminals from either PO or VPM to further suppress the local activation. Selectively recording cell-type-specific calcium signals will provide the possibility to further study the specific role that excitatory/inhibitory neurons play in the mechanism of CC-mediated neuronal activity and neurovascular coupling.

In particular, besides the robust negative modulation detected in the paired O50W and O100W conditions, a refined temporal scale at the O25W condition further demonstrates the CC-mediated inhibitory effect (Supplementary Fig. 12), which can be potentially caused by the $GABA_A$-mediated early IPSP peak elicited by the direct electrical CC stimulation (Kawaguchi 1992). The fact that antidromic activity is not susceptible to the paired optogenetic and whisker stimulation (surely due to weaker ipsilateral whisker-evoked activity, but also likely due to the relative strength of antidromic activation), supports the notion that the depression of whisker-evoked activity is due mainly to local (contralateral) interaction of CC-evoked and whisker-evoked activity, rather than to possible CC activity evoked by indirect activation of additional CPNs via antidromic activation.

The whole-brain fMRI with concurrent calcium recording allows assessing the brain-wide network effects of CC-mediated inhibition (Fig. 4*a*,*b*). In particular, the application of the calcium amplitude-modulation (AM)-based GLM allows separating the stimulus-driven responses from the AM factor, which creates specific correlation maps to the CC-mediated inhibitory effects. The calcium AM-based correlation map highlighted three brain regions: the ventral part of right BC, the left MC, and PO. The ventral right BC was likely activated by reciprocal callosal connections, the majority of which, as argued above, may have been quenched by the strong antidromic effect via labeled CPNs. During the viral injection procedure, however, the ventral BC was regularly spared and did not receive virus, and therefore may have been less affected by overriding antidromic activity. Outside BC on the orthodromic side, the AM2-dependent correlation was detected as well in the left MC and PO. The CC-mediated inhibitory effect on the spatially distinct MC could be caused by the long-range S1-MC projection for sensorimotor integration (Ferezou et al. 2007; Matyas et al. 2010; Kleinfeld and Deschenes 2011; Chen et al. 2013; Feldmeyer et al. 2013). The direct BOLD activation in the MC was detected by whisker stimulation through the sensorimotor connection (Yu et al. 2014), which was also shown in the antidromic activity-based spreading activation patterns (Fig. 1*e*). The CC-mediated inhibitory effect on the PO is likely via corticothalamic projections originating from BC layer 5b neurons (Groh et al. 2014; Mease et al. 2016b, 2016c; Sumser et al. 2017). This could further lead to feed-forward suppression through the PO $\rightarrow$BC thalamocortical circuit. This suggests potential participation of the callosal inputs in the regulation of a wider network of a reciprocal thalamocortical network, which mediates BC signals from the other hemisphere for whisking related processing (Petreanu et al. 2009; Theyel et al. 2010; Feldmeyer et al. 2013; Gambino et al. 2014; Manita et al. 2015; Mease, Metz, et al. 2016a; Sumser et al. 2017). Therefore, besides the antidromically evoked network activation pattern, the orthodromic CC-mediated inhibition generates a brain-wide activity pattern of its own.

In summary, by taking advantage of optogenetics to activate unidirectional callosal fibers, calcium indicators (GCaMP6f) to track neuronal activity at L5, and simultaneous whole-brain fMRI mapping, this work bridges the cellular and the whole brain network levels for CC-mediated activity. We present a multimodal fMRI platform to map and analyze the CC-regulated excitation/inhibition balance across multiple scales, which should be useful to decipher brain network dysfunction induced from CC abnormalities. Brain-wide network activation from callosal-circuit optogenetic stimulation underscores the caution to interpret circuit-specific regulatory mechanisms underlying behavioral or functional outcomes with optogenetics in animals.

Supplementary data

Supplementary materials can be found at *Cerebral Cortex* online.

Author Contributions

X.Y. designed and supervised the research, Y.C. and X.Y. performed animal experiments, Y.C. acquired data, Y.C. analyzed data, A.K., C.S., F.S., and P.P.-R. provided conceptual and technical support, X.Y., Y.C., A.K., and C.S. wrote the manuscript.

Funding

National Institutes of Health (grant 1RF1NS113278), Max-Planck-Society, Deutsche Forschungsgemeinschaft (YU 215/3-1), Bundesministerium für Bildung und Forschung (01GQ1702), National Institutes of Health instrument grant S10 RR023009 to the Massachusetts General Hospital/Harvard-MIT Program in Health Sciences and Technology Martinos Center, the intramural research program of National Institute of Neurological Disorders and Stroke (A. Koretsky), and the China Scholarship Council (Ph.D. fellowship to Y. Chen) are gratefully acknowledged.

Notes

Data generated during this study and related image processing codes are available from the corresponding author upon reasonable request. The Analysis of Functional NeuroImages software (AFNI, NIH, USA) and Matlab (MATLAB, MathWorks, USA) were used to process the fMRI and simultaneously acquired calcium signals, respectively. The relevant source codes can be downloaded through https://afni.nimh.nih.gov/afni/.

We thank Dr R. Pohmann, Dr K. Buckenmaier, Dr N. Avdievitch, Dr J. Engelmann, and Ms H. Schulz for technical support, Dr P. Douay, Mrs R. König, Dr E. Weiler, Ms S. Fischer, and Mrs M. Pitscheider for animal support, the AFNI team for the software support, the Genetically-Encoded Neuronal Indicator and Effector Program and the Janelia Farm Research Campus for kindly providing viral plasmids. *Conflict of Interest:* None declared.

References

Adamantidis AR, Zhang F, Aravanis AM, Deisseroth K, de Lecea L. 2007. Neural substrates of awakening probed with optogenetic control of hypocretin neurons. *Nature*. 450: 420–424.

Albers F, Schmid F, Wachsmuth L, Faber C. 2018a. Line scanning fMRI reveals earlier onset of optogenetically evoked BOLD response in rat somatosensory cortex as compared to sensory stimulation. *Neuroimage*. 164:144–154.

Albers F, Wachsmuth L, van Alst TM, Faber C. 2018b. Multimodal functional neuroimaging by simultaneous BOLD fMRI and Fiber-optic calcium recordings and optogenetic control. *Mol Imaging Biol*. 20:171–182.

Anderson JS, Druzgal TJ, Froehlich A, DuBray MB, Lange N, Alexander AL, Abildskov T, Nielsen JA, Cariello AN, Cooperrider JR, *et al*. 2011. Decreased interhemispheric functional connectivity in autism. *Cereb Cortex*. 21: 1134–1146.

Bernal-Casas D, Lee HJ, Weitz AJ, Lee JH. 2017. Studying brain circuit function with dynamic causal modeling for optogenetic fMRI. *Neuron*. 93:522–532 e525.

Berwick J, Redgrave P, Jones M, Hewson-Stoate N, Martindale J, Johnston D, Mayhew JE. 2004. Integration of neural responses originating from different regions of the cortical somatosensory map. *Brain Res*. 1030:284–293.

Bitzenhofer SH, Ahlbeck J, Wolff A, Wiegert JS, Gee CE, Oertner TG, Hanganu-Opatz IL. 2017. Layer-specific optogenetic activation of pyramidal neurons causes beta-gamma entrainment of neonatal networks. *Nat Commun*. 8:14563.

Bocci T, Caleo M, Giorli E, Barloscio D, Maffei L, Rossi S, Sartucci F. 2011. Transcallosal inhibition dampens neural responses to high contrast stimuli in human visual cortex. *Neuroscience*. 187:43–51.

Boyden ES, Zhang F, Bamberg E, Nagel G, Deisseroth K. 2005. Millisecond-timescale, genetically targeted optical control of neural activity. *Nat Neurosci*. 8:1263–1268.

Butovas S, Hormuzdi SG, Monyer H, Schwarz C. 2006. Effects of electrically coupled inhibitory networks on local neuronal responses to intracortical microstimulation. *J Neurophysiol*. 96:1227–1236.

Butovas S, Schwarz C. 2003. Spatiotemporal effects of microstimulation in rat neocortex: a parametric study using multielectrode recordings. *J Neurophysiol*. 90:3024–3039.

Caminiti R, Carducci F, Piervincenzi C, Battaglia-Mayer A, Confalone G, Visco-Comandini F, Pantano P, Innocenti GM. 2013. Diameter, length, speed, and conduction delay of callosal axons in macaque monkeys and humans: comparing data from histology and magnetic resonance imaging diffusion tractography. *J Neurosci*. 33:14501–14511.

Cardin JA, Carlen M, Meletis K, Knoblich U, Zhang F, Deisseroth K, Tsai LH, Moore CI. 2009. Driving fast-spiking cells induces gamma rhythm and controls sensory responses. *Nature*. 459:663–667.

Cardin JA, Carlen M, Meletis K, Knoblich U, Zhang F, Deisseroth K, Tsai LH, Moore CI. 2010. Targeted optogenetic stimulation and recording of neurons in vivo using cell-type-specific expression of Channelrhodopsin-2. *Nat Protoc*. 5: 247–254.

Carter ME, Yizhar O, Chikahisa S, Nguyen H, Adamantidis A, Nishino S, Deisseroth K, de Lecea L. 2010. Tuning arousal with optogenetic modulation of locus coeruleus neurons. *Nat Neurosci*. 13:1526–1533.

Cauller LJ, Clancy B, Connors BW. 1998. Backward cortical projections to primary somatosensory cortex in rats extend long horizontal axons in layer I. *J Comp Neurol*. 390:297–310.

Chen JL, Carta S, Soldado-Magraner J, Schneider BL, Helmchen F. 2013. Behaviour-dependent recruitment of long-range projection neurons in somatosensory cortex. *Nature*. 499:336–340.

Chen Y, Pais-Roldan P, Chen XM, Frosz MH, Yu X. 2019. MRI-guided robotic arm drives optogenetic fMRI with concurrent Ca^{2+} recording. *Nature Communications*. 10(1): 2536.

Cox RW. 1996. AFNI: software for analysis and visualization of functional magnetic resonance neuroimages. *Comput Biomed Res*. 29:162–173.

Egaas B, Courchesne E, Saitoh O. 1995. Reduced size of corpus callosum in autism. *Arch Neurol*. 52:794–801.

Fame RM, MacDonald JL, Macklis JD. 2011. Development, specification, and diversity of callosal projection neurons. *Trends Neurosci*. 34:41–50.

Feldmeyer D, Brecht M, Helmchen F, Petersen CC, Poulet JF, Staiger JF, Luhmann HJ, Schwarz C. 2013. Barrel cortex function. *Prog Neurobiol*. 103:3–27.

Ferezou I, Haiss F, Gentet LJ, Aronoff R, Weber B, Petersen CC. 2007. Spatiotemporal dynamics of cortical sensorimotor integration in behaving mice. *Neuron*. 56:907–923.

Fox K. 2008. *Barrel Cortex*, Cambridge, UK: Cambridge University Press. ISBN 97-0-521-85217-3.

Gambino F, Pages S, Kehayas V, Baptista D, Tatti R, Carleton A, Holtmaat A. 2014. Sensory-evoked LTP driven by dendritic plateau potentials in vivo. *Nature*. 515:116.

Gao R, Asano SM, Upadhyayula S, Pisarev I, Milkie DE, Liu TL, Singh V, Graves A, Huynh GH, Zhao Y, *et al*. 2019. Cortical column and whole-brain imaging with molecular contrast and nanoscale resolution. *Science*. 363(6424):eaau8302.

Gazzaniga MS. 2000. Cerebral specialization and interhemispheric communication: does the corpus callosum enable the human condition? *Brain*. 123(Pt 7):1293–1326.

Gazzaniga MS. 2005. Forty-five years of split-brain research and still going strong. *Nat Rev Neurosci*. 6:653–659.

Grandjean J, Corcoba A, Kahn MC, Upton AL, Deneris ES, Seifritz E, Helmchen F, Mann EO, Rudin M, Saab BJ. 2019. A brain-wide functional map of the serotonergic responses to acute stress and fluoxetine. *Nat Commun*. 10(1):350.

Groh A, Bokor H, Mease RA, Plattner VM, Hangya B, Stroh A, Deschenes M, Acsady L. 2014. Convergence of cortical and sensory driver inputs on single thalamocortical cells. *Cereb Cortex*. 24:3167–3179.

He Y, Wang M, Chen X, Pohmann R, Polimeni JR, Scheffler K, Rosen BR, Kleinfeld D, Yu X. 2018. Ultra-slow single-vessel BOLD and CBV-based fMRI spatiotemporal dynamics and their correlation with neuronal intracellular calcium signals. *Neuron*. 97:925–939 e925.

Hoffmeyer HW, Enager P, Thomsen KJ, Lauritzen MJ. 2007. Nonlinear neurovascular coupling in rat sensory cortex by activation of transcallosal fibers. *J Cereb Blood Flow Metab*. 27:575–587.

Innocenti GM, Ansermet F, Parnas J. 2003. Schizophrenia, neurodevelopment and corpus callosum. *Mol Psychiatry*. 8:261–274.

Inoue KI, Takada M, Matsumoto M. 2015. Neuronal and behavioural modulations by pathway-selective optogenetic stimulation of the primate oculomotor system. *Nat Commun*. 6:8378.

Iordanova B, Vazquez A, Kozai TD, Fukuda M, Kim SG. 2018. Optogenetic investigation of the variable neurovascular coupling along the interhemispheric circuits. *J Cereb Blood Flow Metab*. 38:627–640.

Just N, Faber C. 2019. Probing activation-induced neurochemical changes using optogenetics combined with functional magnetic resonance spectroscopy: a feasibility study in the rat primary somatosensory cortex. *J Neurochem*. 150:402–419.

Karayannis T, Huerta-Ocampo I, Capogna M. 2007. GABAergic and pyramidal neurons of deep cortical layers directly receive and differently integrate callosal input. *Cereb Cortex*. 17:1213–1226.

Karolis VR, Corbetta M, Thiebaut de Schotten M. 2019. The architecture of functional lateralisation and its relationship to callosal connectivity in the human brain. *Nat Commun*. 10:1417.

Kawaguchi Y. 1992. Receptor subtypes involved in callosally-induced postsynaptic potentials in rat frontal agranular cortex in vitro. *Exp Brain Res*. 88:33–40.

Kim CK, Adhikari A, Deisseroth K. 2017. Integration of optogenetics with complementary methodologies in systems neuroscience. *Nat Rev Neurosci*. 18:222–235.

Kleinfeld D, Deschenes M. 2011. Neuronal basis for object location in the vibrissa scanning sensorimotor system. *Neuron*. 72:455–468.

Kumar SS, Huguenard JR. 2001. Properties of excitatory synaptic connections mediated by the corpus callosum in the developing rat neocortex. *J Neurophysiol*. 86:2973–2985.

Lee AT, Gee SM, Vogt D, Patel T, Rubenstein JL, Sohal VS. 2014. Pyramidal neurons in prefrontal cortex receive subtype-specific forms of excitation and inhibition. *Neuron*. 81:61–68.

Lee JH, Durand R, Gradinaru V, Zhang F, Goshen I, Kim DS, Fenno LE, Ramakrishnan C, Deisseroth K. 2010. Global and local fMRI signals driven by neurons defined optogenetically by type and wiring. *Nature*. 465:788–792.

Li X, Gutierrez DV, Hanson MG, Han J, Mark MD, Chiel H, Hegemann P, Landmesser LT, Herlitze S. 2005. Fast noninvasive activation and inhibition of neural and network activity by vertebrate rhodopsin and green algae channelrhodopsin. *Proc Natl Acad Sci U S A*. 102:17816–17821.

Lima SQ, Miesenbock G. 2005. Remote control of behavior through genetically targeted photostimulation of neurons. *Cell*. 121:141–152.

Logothetis NK, Augath M, Murayama Y, Rauch A, Sultan F, Goense J, Oeltermann A, Merkle H. 2010. The effects of electrical microstimulation on cortical signal propagation. *Nat Neurosci*. 13:1283–1291.

Manita S, Suzuki T, Homma C, Matsumoto T, Odagawa M, Yamada K, Ota K, Matsubara C, Inutsuka A, Sato M, *et al*. 2015. A top-down cortical circuit for accurate sensory perception. *Neuron*. 86:1304–1316.

Matyas F, Sreenivasan V, Marbach F, Wacongne C, Barsy B, Mateo C, Aronoff R, Petersen CC. 2010. Motor control by sensory cortex. *Science*. 330:1240–1243.

Mease RA, Metz M, Groh A. 2016a. Cortical sensory responses are enhanced by the higher-order thalamus. *Cell Rep*. 14:208–215.

Mease RA, Sumser A, Sakmann B, Groh A. 2016b. Cortical dependence of whisker responses in posterior medial thalamus in vivo. *Cereb Cortex*. 26:3534–3543.

Mease RA, Sumser A, Sakmann B, Groh A. 2016c. Corticothalamic spike transfer via the L5B-POm pathway in vivo. *Cereb Cortex*. 26:3461–3475.

Mitchell BD, Macklis JD. 2005. Large-scale maintenance of dual projections by callosal and frontal cortical projection neurons in adult mice. *J Comp Neurol*. 482:17–32.

Moore CI, Carlen M, Knoblich U, Cardin JA. 2010. Neocortical interneurons: from diversity, strength. *Cell*. 142:189–193.

Nagel G, Brauner M, Liewald JF, Adeishvili N, Bamberg E, Gottschalk A. 2005. Light activation of channelrhodopsin-2 in excitable cells of Caenorhabditis elegans triggers rapid behavioral responses. *Curr Biol*. 15:2279–2284.

Nagel G, Ollig D, Fuhrmann M, Kateriya S, Musti AM, Bamberg E, Hegemann P. 2002. Channelrhodopsin-1: a light-gated proton channel in green algae. *Science*. 296:2395–2398.

Nemoto M, Hoshi Y, Sato C, Iguchi Y, Hashimoto I, Kohno E, Hirano T, Terakawa S. 2012. Diversity of neural-hemodynamic relationships associated with differences in cortical processing during bilateral somatosensory activation in rats. *Neuroimage*. 59:3325–3338.

Ni Z, Gunraj C, Nelson AJ, Yeh IJ, Castillo G, Hoque T, Chen R. 2009. Two phases of interhemispheric inhibition between motor related cortical areas and the primary motor cortex in human. *Cereb Cortex*. 19:1654–1665.

Ogawa S, Lee TM, Stepnoski R, Chen W, Zhu XH, Ugurbil K. 2000. An approach to probe some neural systems interaction by functional MRI at neural time scale down to milliseconds. *Proc Natl Acad Sci U S A*. 97:11026–11031.

Palmer LM, Schulz JM, Larkum ME. 2013. Layer-specific regulation of cortical neurons by interhemispheric inhibition. *Commun Integr Biol*. 6:e23545.

Palmer LM, Schulz JM, Murphy SC, Ledergerber D, Murayama M, Larkum ME. 2012. The cellular basis of GABA(B)-mediated interhemispheric inhibition. *Science*. 335:989–993.

Petreanu L, Huber D, Sobczyk A, Svoboda K. 2007. Channelrhodopsin-2-assisted circuit mapping of long-range callosal projections. *Nat Neurosci*. 10:663–668.

Petreanu L, Mao T, Sternson SM, Svoboda K. 2009. The subcellular organization of neocortical excitatory connections. *Nature*. 457:1142–1145.

Petrus E, Saar G, Ma Z, Dodd S, Isaac JTR, Koretsky AP. 2019. Interhemispheric plasticity is mediated by maximal potentiation of callosal inputs. *Proc Natl Acad Sci U S A*. 116: 6391–6396.

Pomarol-Clotet E, Canales-Rodriguez EJ, Salvador R, Sarro S, Gomar JJ, Vila F, Ortiz-Gil J, Iturria-Medina Y, Capdevila A, McKenna PJ. 2010. Medial prefrontal cortex pathology in schizophrenia as revealed by convergent findings from multimodal imaging. *Mol Psychiatry*. 15:823–830.

Rock C, Apicella AJ. 2015. Callosal projections drive neuronal-specific responses in the mouse auditory cortex. *J Neurosci*. 35:6703–6713.

Rock C, Zurita H, Lebby S, Wilson CJ, Apicella AJ. 2018. Cortical circuits of Callosal GABAergic neurons. *Cereb Cortex*. 28:1154–1167.

Ryali S, Shih YY, Chen T, Kochalka J, Albaugh D, Fang Z, Supekar K, Lee JH, Menon V. 2016. Combining optogenetic stimulation and fMRI to validate a multivariate dynamical systems model for estimating causal brain interactions. *Neuroimage*. 132:398–405.

Schaefer GB, Bodensteiner JB. 1999. Developmental anomalies of the brain in mental retardation. *Int Rev Psychiatr*. 11:47–55.

Schmid F, Wachsmuth L, Schwalm M, Prouvot PH, Jubal ER, Fois C, Pramanik G, Zimmer C, Faber C, Stroh A. 2016. Assessing sensory versus optogenetic network activation by combining (o)fMRI with optical Ca^{2+} recordings. *J Cereb Blood Flow Metab*. 36:1885–1900.

Schnitzler A, Kessler KR, Benecke R. 1996. Transcallosally mediated inhibition of interneurons within human primary motor cortex. *Exp Brain Res*. 112:381–391.

Schulte T, Muller EM, Oehring EM. 2010. Contribution of callosal connections to the interhemispheric integration of visuomotor and cognitive processes. *Neuropsychol Rev*. 20: 174–190.

Schulz K, Sydekum E, Krueppel R, Engelbrecht CJ, Schlegel F, Schroter A, Rudin M, Helmchen F. 2012. Simultaneous BOLD fMRI and fiber-optic calcium recording in rat neocortex. *Nat Methods*. 9:597–602.

Schwalm M, Schmid F, Wachsmuth L, Backhaus H, Kronfeld A, Aedo Jury F, Prouvot PH, Fois C, Albers F, van Alst T, *et al*. 2017. Cortex-wide BOLD fMRI activity reflects locally-recorded slow oscillation-associated calcium waves. *Elife*. 6:e27602

Shuler MG, Krupa DJ, Nicolelis MA. 2001. Bilateral integration of whisker information in the primary somatosensory cortex of rats. *J Neurosci*. 21:5251–5261.

Simmons PA, Pearlman AL. 1983. Receptive-field properties of transcallosal visual cortical neurons in the normal and reeler mouse. *J Neurophysiol*. 50:838–848.

Spencer SS, Spencer DD, Williamson PD, Sass K, Novelly RA, Mattson RH. 1988. Corpus callosotomy for epilepsy. 1. Seizure effects. *Neurology*. 38:19–24.

Sperry RW. 1961. Cerebral organization and behavior: the split brain behaves in many respects like two separate brains, providing new research possibilities. *Science*. 133:1749–1757.

Suarez R, Fenlon LR, Marek R, Avitan L, Sah P, Goodhill GJ, Richards LJ. 2014. Balanced interhemispheric cortical activity is required for correct targeting of the corpus callosum. *Neuron*. 82:1289–1298.

Sumser A, Mease RA, Sakmann B, Groh A. 2017. Organization and somatotopy of corticothalamic projections from L5B in mouse barrel cortex. *Proc Natl Acad Sci U S A*. 114:8853–8858.

Sych Y, Chernysheva M, Sumanovski LT, Helmchen F. 2019. High-density multi-fiber photometry for studying large-scale brain circuit dynamics. *Nat Methods*. 16:553–560.

Theyel BB, Llano DA, Sherman SM. 2010. The corticothalamocortical circuit drives higher-order cortex in the mouse. *Nat Neurosci*. 13:84–88.

Tsai HC, Zhang F, Adamantidis A, Stuber GD, Bonci A, de Lecea L, Deisseroth K. 2009. Phasic firing in dopaminergic neurons is sufficient for behavioral conditioning. *Science*. 324:1080–1084.

Tye KM, Deisseroth K. 2012. Optogenetic investigation of neural circuits underlying brain disease in animal models. *Nat Rev Neurosci*. 13:251–266.

van Alst TM, Wachsmuth L, Datunashvili M, Albers F, Just N, Budde T, Faber C. 2019. Anesthesia differentially modulates neuronal and vascular contributions to the BOLD signal. *Neuroimage*. 195:89–103.

van Eijsden P, Otte WM, van der Hel WS, van Nieuwenhuizen O, Dijkhuizen RM, de Graaf RA, Braun KP. 2011. In vivo diffusion tensor imaging and ex vivo histologic characterization of white matter pathology in a post-status epilepticus model of temporal lobe epilepsy. *Epilepsia*. 52:841–845.

van Schooneveld MM, Jennekens-Schinkel A, van Rijen PC, Braun KP, van Nieuwenhuizen O. 2011. Hemispherectomy: a basis for mental development in children with epilepsy. *Epileptic Disord*. 13:47–55.

Veinante P, Deschenes M. 2003. Single-cell study of motor cortex projections to the barrel field in rats. *J Comp Neurol*. 464:98–103.

Wang M, He Y, Sejnowski TJ, Yu X. 2018. Brain-state dependent astrocytic Ca(2+) signals are coupled to both positive and negative BOLD-fMRI signals. *Proc Natl Acad Sci U S A*. 115:E1647–E1656.

White EL, Czeiger D. 1991. Synapses made by axons of callosal projection neurons in mouse somatosensory cortex—emphasis on intrinsic connections. *J Comp Neurol*. 303:233–244.

Wiest MC, Bentley N, Nicolelis MA. 2005. Heterogeneous integration of bilateral whisker signals by neurons in primary somatosensory cortex of awake rats. *J Neurophysiol*. 93:2966–2973.

Wilson CJ. 1987. Morphology and synaptic connections of crossed corticostriatal neurons in the rat. *J Comp Neurol*. 263:567–580.

Xin Yu SD, Koretsky AP. 2013. Targeting projection fibers for optogenetics and fMRI. In 21st Annual Meeting and Exhibition of the International Society for Magnetic Resonance in Medicine (ISMRM 2013).

Yu X, Chung S, Chen DY, Wang S, Dodd SJ, Walters JR, Isaac JT, Koretsky AP. 2012. Thalamocortical inputs show post-critical-period plasticity. *Neuron*. 74:731–742.

Yu X, He Y, Wang M, Merkle H, Dodd SJ, Silva AC, Koretsky AP. 2016. Sensory and optogenetically driven single-vessel fMRI. *Nat Methods*. 13:337–340.

Yu X, Qian C, Chen DY, Dodd SJ, Koretsky AP. 2014. Deciphering laminar-specific neural inputs with line-scanning fMRI. *Nat Methods*. 11:55–58.

Zhang F, Wang LP, Boyden ES, Deisseroth K. 2006. Channelrhodopsin-2 and optical control of excitable cells. *Nat Methods*. 3:785–792.